Outer Hair Cell Somatic Electromotility In Vivo and Power Transfer to the Organ of Corti

Sripriya Ramamoorthy[†] and Alfred L. Nuttall[†‡*]
[†]Oregon Hearing Research Center, Department of Otolaryngology, Oregon Health & Science University, Portland, Oregon; and [‡]Kresge Hearing Research Institute, University of Michigan, Ann Arbor, Michigan

ABSTRACT The active amplification of sound-induced vibrations in the cochlea, known to be crucial for auditory sensitivity and frequency selectivity, is not well understood. The outer hair cell (OHC) somatic electromotility is a potential mechanism for such amplification. Its effectiveness in vivo is putatively limited by the electrical low-pass filtering of the cell's transmembrane potential. However, the transmembrane potential is an incomplete metric. We propose and estimate two metrics to evaluate the effectiveness of OHC electromotility in vivo. One metric is the OHC electromechanical ratio defined as the amplitude of the ratio of OHC displacement to the change in its transmembrane potential. The in vivo electromechanical ratio is derived from the recently measured in vivo displacements of the reticular lamina and the basilar membrane at the 19 kHz characteristic place in guinea pigs and using a model. The ratio, after accounting for the differences in OHC vibration in situ due to the impedances from the adjacent structures, is in agreement with the literature values of the in vitro electromechanical ratio measured by others. The second and more insightful metric is the OHC somatic power. Our analysis demonstrates that the organ of Corti is nearly optimized to receive maximum somatic power in vivo and that the estimated somatic power could account for the active amplification.

INTRODUCTION

Normal hearing depends on sound amplification in the mammalian cochlea. The sound entering the ear stimulates the cochlea and launches a fluid-structure traveling wave along the cellular structures. It has been hypothesized (1,2) that an active process adds biochemical energy to the traveling wave by applying feedback forces that amplify and fine-tune the cellular vibrations (3,4). These amplified and fine-tuned vibrations deflect the hair bundles (HBs) of the inner hair cells, which send signals to the brain via the auditory neurons. The fine-tuning and amplification are crucial for our normal sensitive hearing. However, the details of the hypothesized feedback process are still under investigation (5). Two potential force-producing candidates are outer hair cell (OHC) electromotility and HB motility (5–7). Many indirect studies have supported either mechanism or both (8,9), but the issue remains unresolved. It is important to resolve this issue because sensorineural hearing loss begins with deterioration of the active process.

OHCs are essential for cochlear amplification (6). Voltage-dependent changes in OHC length have been demonstrated in isolated cells (10) and the phenomenon is reciprocal and indicative of piezoelectricity (11). In vitro, the OHCs have been found to demonstrate dynamic length changes at least until 79 kHz (12). However, the ability of the electromotility mechanism to influence the organ mechanics in vivo has been challenged by the relatively long membrane time constant (RC) of the hair cell, which is expected to attenuate alternating transmembrane potentials at frequencies above a kilohertz (13), although, electrically induced organ of Corti (OoC) motion is seen to 100 kHz in vivo (14). Many possible solutions to this time constant problem have been proposed. For example, Gummer et al. (15) has experimentally demonstrated tectorial membrane (TM) shear resonance in apical guinea pig measurement, which if extended to basal regions could compensate for the time constant problem. Lu et al. (16) suggested that analogous to the gain-bandwidth product for operational amplifiers, the OHC amplifier's collective gain could be traded off for larger bandwidth via negative feedback and thereby increase the cutoff frequency of the low-pass filter. Dallos and Evans (17) postulated that the extracellular potential in the space surrounding the OHCs could be sufficient to drive the OHC at frequencies up to 22 kHz. Significant and tuned extracellular potentials were measured by Fridberger et al. (18) in the space surrounding the OHC in vivo in the basal turn in guinea pigs. Liao et al. (19) estimated the active force due to electromotility to be sufficient despite the RC filtering, but their study was limited by the unavailability of simultaneous in vivo measurements of the reticular lamina (RL) and basilar membrane (BM) displacements. These and other solutions proposed so far are summarized by Dallos ((5), p. 7).

It is important to note that smaller OHC time constant per se does not result in larger transmembrane potentials, whereas larger transduction current (which is due to stimulus-induced modulation of a standing current (20)) does. Large standing currents and their modulation (20) on the order of 500 pA were shown by in vivo current density analysis (21). The large transduction current has been recently

Submitted August 19, 2011, and accepted for publication December 23, 2011.

*Correspondence: nuttall@ohsu.edu

Editor: Richard Bertram.

0006-3495/12/02/0388/11 $2.00

doi: 10.1016/j.bpj.2011.12.040

confirmed for isolated OHCs when the in vivo ionic environment is replicated (22). However, as Ashmore (23) points out, measurements have not been made from cells of the high-frequency region of the cochlea.

We do not propose how the low-pass filtering of the OHC transmembrane potential may be compensated. Instead, we propose that the transmembrane potential considered independently is not sufficient to assess the effectiveness of OHC electromotility in vivo because the level of the transmembrane potential needed for active amplification in the cochlea is unknown and ill-defined. We propose and evaluate two metrics for the effectiveness of the OHC electromotility in vivo at low stimulus levels. One metric is the OHC electromechanical ratio defined as the amplitude of the ratio of OHC displacement to the change in its transmembrane potential. In isolated OHCs, this ratio is the same as the piezoelectric coefficient. Another more insightful metric is the OHC somatic power in vivo. We predict its effectiveness to influence the vibrations of the OoC structures and evaluate how it compares with an estimate of the active power in BM vibrations.

First, the relationship between in vivo OHC displacement to isolated OHC displacement for a given change in the transmembrane potential is derived based on theoretical modeling. Insights on somatic power transfer to the OoC are derived from the model. It is commonly assumed that the somatic force is nearly isometric in vivo due to the impedances imposed on the OHC by the surrounding tissues (6,24,25). Recently, Rabbitt et al. (26) (based on an OHC piezoelectric model) suggested that the power efficiency of OHC electromotility would require the OoC to be impedance matched with the OHC. They did not show if that is the case in vivo. Here, we show that the OoC in vivo is nearly impedance matched with the OHC and would therefore receive maximum somatic power. Second, the acoustically evoked OHC displacement and HB displacement are estimated from recent in vivo measurements (27) of RL and BM motion at 40 dB SPL in sensitive anesthetized guinea pigs at the 19 kHz characteristic frequency (CF) in the basal turn. The HB transduction current and the OHC transmembrane potential are then estimated. The in vivo OHC electromechanical ratio is compared with the ratio in isolated cells around the 19 kHz characteristic place (CP). The somatic power for this stimulus is predicted and compared with the average power of BM vibrations versus the input power at the stapes.

METHODS

Electromechanical ratio as a metric to evaluate the effectiveness of OHC electromotility

The OHC electromechanical ratio is defined as

$$EMR = \left|\frac{u_{OHC}}{\Delta\varphi_{OHC}}\right|, \tag{1}$$

where the numerator is the OHC displacement and the denominator is the OHC transmembrane potential in response to low level sound stimulation below and up to ~40 dB SPL. Based on whole cell voltage clamp measurements on isolated OHCs (28,29), the EMR in isolated cells is given by

$$EMR_{iso} = \left|\frac{u_{OHC}^{iso}}{\Delta\varphi_{OHC}}\right|_{measured} \approx 20\ \text{nm/mV}. \tag{2}$$

The EMR in isolated cells, EMR_{iso}, which is the same as its piezoelectric coefficient, characterizes the OHC electromotility. Therefore, in this article, the EMR is evaluated in vivo to assess the effectiveness of OHC electromotility in the basal region in guinea pigs at low sound stimulus levels.

In vivo, two factors are important to consider. First, in response to a change in the transmembrane potential, the electromechanical displacement of the OHC in vivo is not the same as that in isolated cells. In situ and in vivo, the OHCs are a part of the cochlear partition and thus their vibration is tied to the vibrations of the rest of the structures. Second, the OHC transmembrane potential in vivo is hypothesized to be small at near-CF frequencies at basal locations due to RC low-pass filtering with cutoff below a kHz (5,13,30). A recent study (22) reports significantly higher cutoff frequencies for this low-pass filter than reported earlier, but the issue remains unsettled.

Somatic power as a metric to evaluate the effectiveness of OHC electromotility

The active amplification in the cochlea would be most directly addressed by evaluating the active power, if any, imparted to the OoC structures by the active process (in this case, the OHC electromotility). The power referred to here is temporally averaged as well as integrated over a spatial region.

The power due to OHC somatic electromotility in vivo is given by

$$P_{somatic} = \frac{1}{2}\text{Real}(Z_{somatic})|(j\omega u_{OHC})|^2. \tag{3}$$

Here, $Z_{somatic}$ is the impedance (units Ns/m) seen by the somatic force in vivo, ω is the radial stimulus frequency, and u_{OHC} is the OHC displacement.

It is expected that the acoustic power input to the cochlea as well as any power from active sources inside the cochlea would be dissipated due to damping. Strictly speaking, the cycle-averaged power in BM vibrations should be spatially integrated over the whole extent of the traveling wave. However, due to the significant slowing of the traveling wave near the best place, most of the power is expected to be dissipated around the best place (31). In this work, the average power is estimated over one wavelength around the best place. At high stimulus levels >100 dB SPL, where cochlear amplification is negligible, it is expected that the average power in BM vibrations would be less than or at most equal to the average power input at the stapes. At low stimulus levels, <~40 dB SPL, the average power in BM vibrations may be expected to be higher than the power input at the stapes if active power is added to the traveling wave. (Note that earlier modeling efforts and experimental estimates have supported active power addition to the traveling wave at low stimulus levels; see for example (32–34.)

The average power in BM vibrations is equal to the power dissipated by BM, and is given by

$$P_{BM} = \frac{1}{2}B_{BM}|(j\omega u_{BM})|^2. \tag{4}$$

Here, B_{BM} is the BM damping coefficient (units Ns/m), ω is the radial stimulus frequency, and u_{BM} is BM displacement.

The acoustic power input to the cochlea at the stapes is given by

$$P_{stapes} = \frac{1}{2}\text{Real}(Z_C)|(j\omega u_{st})|^2. \quad (5)$$

Here, Z_C is the cochlear input impedance (units Ns/m) at the stapes, ω is the radial stimulus frequency, and u_{ST} is the stapes displacement at a certain stimulus level and frequency.

The predicted somatic power $P_{somatic}$ is compared with $(P_{BM} - P_{stapes})$ to assess whether the electromotility could account for the active power (if any) in BM vibrations at low stimulus levels. Furthermore, the effectiveness of somatic power transfer to the OoC is evaluated using a lumped two-mass model.

RESULTS

Model for OHC electromotility in vivo versus isolated cells

The displacement of the OHC in vivo in response to a change in its transmembrane potential is constrained by the impedance of the BM at the basal pole and by the RL-TM complex at the apical pole. The effect of these mechanical constraints on the resulting OHC electromechanical displacement is modeled in this section. At low sound stimulus levels (<40 dB SPL) it is assumed that the response due to the active force dominates over passive forces around the CP.

The OHC piezoelectric behavior is, strictly speaking, nonlinear and as described by Dong et al. (in Eq. 1 and Eq. 2 in (11); see also (35)). The mechanics of OHC electromotility can be represented by linearized approximation appropriate for low stimulus levels (36) as

$$F_{OHC} = K_{OHC}u_{OHC} + \varepsilon\Delta\varphi_{OHC}. \quad (6)$$

Here, F_{OHC} is the net force applied by the OHC on its apical and basal ends. The first term on the right side of Eq. 6 is the passive force due to the stiffness of the OHC, and the second term is the active force arising due to the change in OHC transmembrane potential. The quantity K_{OHC} is the axial stiffness, u_{OHC} is the in vivo OHC displacement due to electromotility, ε is the electromechanical coupling coefficient (a negative quantity equal to −0.1 nN/mV for a single cell (37), and $\Delta\varphi_{OHC}$ is the a.c. transmembrane potential of the OHC (depolarization is positive).

An isolated OHC is effectively unloaded; that is, in Eq. 6, $F_{OHC} = 0$ for isolated cells. Therefore, the displacement of an isolated OHC due to applied transmembrane potential is given by

$$u_{OHC}^{iso} = -\frac{\varepsilon\Delta\varphi_{OHC}}{K_{OHC}}. \quad (7)$$

Using Eq. 7, Eq. 6 can be rewritten as

$$F_{OHC} = K_{OHC}\left(u_{OHC} - u_{OHC}^{iso}\right). \quad (8)$$

The somatic force acts on the cochlear partition in the manner described in Fig. 1 *A* (oriented toward scala vestibuli (SV) on the RL/TM complex and toward scala tympani (ST) on the BM), and is given by

$$F_{OHC}^{active} = -K_{OHC}u_{OHC}^{iso} = \varepsilon\Delta\varphi_{OHC}. \quad (9)$$

For a depolarizing transmembrane potential or positive $\Delta\varphi_{OHC}$, the active force F_{OHC}^{active} shown in Fig. 1 *A* is negative (because u_{OHC}^{iso} is positive or equivalently because ε is negative), thus pulling the RL/TM complex toward ST and the BM toward SV.

OoC response to OHC somatic force in vivo

The equivalent mechanical representation of the OoC micromechanics adopted from the mechanical representation of the two-mass model of a section of the OoC in Fig. 1 *C* of Markin and Hudspeth (38) (also used in (16,39)), is shown here in Fig. 1 *A*. It is important to note that Fig. 1 *A* is consistent with the OHC represented as a motile element in series with a stiffness element, consistent with Iwasa and Adachi (37). The active displacement in isolated OHC shown by Δl in Fig. 1 *C* in Markin and Hudspeth (38); or by Δz_m in Fig. 8 *B* in Iwasa and Adachi (37) is the same as u_{OHC}^{iso} in this article.

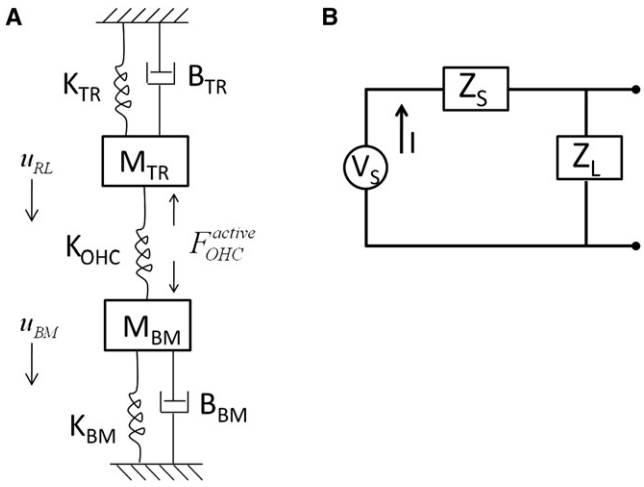

FIGURE 1 (*A*) Lumped mechanical representation of a cross section of the cochlear partition. The active force F_{OHC}^{active} due to OHC electromotility acts on the RL-TM complex (represented as TR) at the apical pole of the OHC and on the BM at the basal OHC pole. In this figure, K represents stiffness, M is the mass, and B is the viscous damping coefficient of the respective structures. The displacements of BM and RL due to the active force are u_{BM} and u_{RL} toward the ST. (*B*) Thévenin equivalent circuit for a generic electrical circuit showing a voltage source V_S with source impedance Z_S and load impedance Z_L. From panel (*A*), the active somatic force is analogous to the voltage source, the OHC self-impedance is equivalent to the source impedance, OHC velocity is analogous to the current *I*, and the combined impedance of BM and RL/TM is equivalent to the load impedance.

Based on the mechanical representation, the following governing equations for the OoC micromechanics in response to only OHC somatic force excitation are derived at steady state and as a function of frequency:

$$Z_{TR}u_{RL} + K_{OHC}(u_{RL} - u_{BM}) = -F_{OHC}^{active}, \quad (10)$$

$$Z_{BM}u_{BM} + K_{OHC}(u_{BM} - u_{RL}) = F_{OHC}^{active}. \quad (11)$$

In Eq. 10 and Eq. 11, $Z_{TR} = (K_{TR} - \omega^2 M_{TR}) + j\omega B_{TR}$ is the impedance of the RL-TM complex, and $Z_{BM} = (K_{BM} - \omega^2 M_{BM}) + j\omega B_{BM}$ is the impedance of the BM, and include the fluid mass loading on the structures. Here, K_{TR} is the stiffness, M_{TR} is the mass including fluid loading (if any), and B_{TR} is the viscous damping coefficient of the RL/TM complex; K_{BM} is BM stiffness, B_{BM} is its viscous damping coefficient, and M_{BM} is the mass of the BM and includes the mass due to fluid loading. The lumped impedance parameters are evaluated over one wavelength near the CP (see legend for Fig. 2, Fig. 3).

Summing Eq. 10 and Eq. 11 gives

$$u_{RL} = -\frac{Z_{BM}}{Z_{TR}}u_{BM}. \quad (12)$$

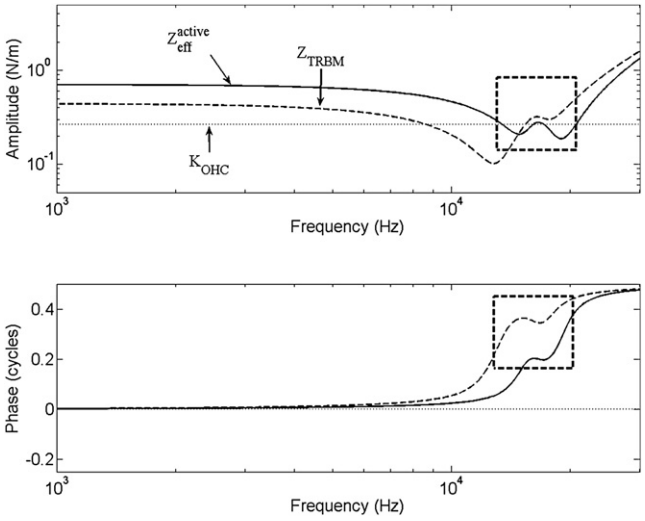

FIGURE 2 Effective impedance of the OoC Z_{eff}^{active} as seen by the OHC somatic force is shown (*solid line*) along with the combined impedance of the BM and the RL/TM complex (Z_{TRBM}; *dashed line*), and the OHC (K_{OHC}; *dotted line*). At frequencies below 12 kHz and above 20 kHz, the effective impedance of the OoC is much higher than the OHC stiffness. However, around 14–20 kHz (*boxed region*) the internal resonances in the OoC reduce Z_{eff}^{active} bringing it down to the level of K_{OHC}. Furthermore, the load impedance is approximately conjugate matched to the source impedance, approaching the maximum power transfer condition; see text for details. Here, $K_{OHC} = 0.265$ N/m lumped over 300 μm, $K_{BM} = 10\,K_{OHC}$, $K_{TR} = 2K_{OHC}$, $M_{BM} = K_{BM}/\omega_{BM}^2$; $\omega_{BM} = 2\pi f_{BM}$; $f_{BM} = 17.5$ kHz; $M_{TR} = K_{TR}/\omega_{TR}^2$; $\omega_{TR} = 2\pi f_{TR}$; $f_{TR} = 13$ kHz, $B_{BM} = 2\zeta_{BM}\sqrt{M_{BM}K_{BM}}$ (for $\zeta_{BM} = 0.1$), and $B_{TR} = 2\zeta_{TR}\sqrt{M_{TR}K_{TR}}$ (for $\zeta_{TR} = 0.1$). For parameter details, please refer to Fig. 3 legend.

Substituting Eq. 12 into Eq. 11, the displacement of BM and RL toward the ST are given by

$$u_{BM} = \frac{F_{OHC}^{active}}{K_{OHC} + \dfrac{Z_{TR}Z_{BM}}{Z_{TR} + Z_{BM}}}\frac{Z_{TR}}{Z_{TR} + Z_{BM}}, \quad (13)$$

$$u_{RL} = \frac{-F_{OHC}^{active}}{K_{OHC} + \dfrac{Z_{TR}Z_{BM}}{Z_{TR} + Z_{BM}}}\frac{Z_{BM}}{Z_{TR} + Z_{BM}}. \quad (14)$$

The OHC displacement in vivo due to the active force F_{OHC}^{active} is given by the difference between the RL and BM displacements from Eq. 13 and Eq. 14 as (ignoring here a factor of ~0.87 due to RL tilt relative to the vertical):

$$u_{OHC} = u_{RL} - u_{BM} = \frac{-F_{OHC}^{active}}{K_{OHC} + \dfrac{Z_{TR}Z_{BM}}{Z_{TR} + Z_{BM}}}. \quad (15)$$

OoC is nearly optimized to receive maximum somatic power

The effective impedance of the OoC (Fig. 2) as seen by the OHC active force is given by (denominator in Eq. 15):

$$Z_{eff}^{active} = K_{OHC} + \frac{Z_{TR}Z_{BM}}{Z_{TR} + Z_{BM}}. \quad (16)$$

Note that $Z_{eff}^{active} = j\omega\, Z_{somatic}$ and has the units of N/m. This effective impedance is a parallel combination of the OHC stiffness with a series combination of RL/TM complex and BM (which includes the fluid mass loading on the BM). The frequency response of this impedance for the 3 mm tonotopic location is shown in Fig. 2. At low frequencies, the effective impedance shown by the solid line is mostly influenced by the impedances of RL/TM and the OHC stiffness. Starting from nearly 12 kHz in Fig. 2 and until ~20 kHz, all the impedances, including that of the BM, influence the effective impedance. The internal resonances of the OoC cause amplitude minima in the impedance around 14–20 kHz in Fig. 2. The double minima in Fig. 2 arise out of two internal resonances because of two masses used in the lumped mechanical representation.

The active power due to electromotility, averaged over one cycle, is given by (an alternative but equivalent expression is given in the Methods section):

$$P_{somatic} = \frac{1}{2}\mathrm{Re}\{(-F_{OHC}^{active})(j\omega u_{OHC})^*\}, \quad (17)$$

where the superscript * indicates complex conjugate. Based on analogy with the classical electrical circuit theory

(Thévenin equivalent circuit shown in Fig.1 *B*) maximum power transfer from the source V_S to the load impedance Z_L occurs when the load impedance is the complex conjugate of the source impedance Z_S (that is, $Z_L^* = Z_S$). In the lumped mechanical representation shown in Fig. 1 *A*, the somatic force is analogous to the voltage source; the OHC velocity is analogous to the current drawn at the source, $K_{OHC}/j\omega$ is the source impedance, and $1/j\omega\, Z_{TR}Z_{BM}/Z_{TR} + Z_{BM}$ is the load impedance. Therefore, for maximum active power transfer to the OoC, the condition to be satisfied is

$$\left(\frac{1}{j\omega}\frac{Z_{TR}Z_{BM}}{Z_{TR}+Z_{BM}}\right)^* = \frac{1}{j\omega}K_{OHC}. \tag{18}$$

This is equivalent to

$$\left(\frac{Z_{TR}Z_{BM}}{Z_{TR}+Z_{BM}}\right)^* = -K_{OHC}.$$

This condition is approximately satisfied around 14 to 20 kHz in Fig. 2, which uses $K_{BM} = 10\ K_{OHC}$, $K_{TR} = K_{BM}/5$. In the spatial domain, applying tonotopic mapping, this frequency range translates to just basal to the CP, consistent with the classical notion (32) of power insertion in this spatial region. From Fig. 2, $(Z_{TR}Z_{BM}/Z_{TR}+Z_{BM})^* \approx (-1-0.71\,\mathrm{j})K_{OHC}$ in that frequency range. Without the OoC internal resonances, such an impedance matching would not occur in the OoC as evident from the low-frequency and high-frequency impedances in Fig. 2. The degree of quantitative matching of the impedances does depend on the parameter values used for stiffness and mass (see the legend for Fig. 2, Fig. 3). For example, $K_{BM} = 50\,K_{OHC},\ K_{TR} = 10\,K_{OHC}(Z_{TR}Z_{BM}/Z_{TR}+Z_{BM})^* \approx (-2.8-3.3\,\mathrm{j})K_{OHC}$ around 15 kHz. However, note that for maximum active force to be applied on the OoC structures the load impedance would be infinite—such a load would receive significantly smaller power from the active process. The lumped mechanical representation of the OoC suggests approximately matched rather than infinite load impedance, and hence supports maximum somatic power transfer to the OoC rather than maximum somatic force applied to the OoC structures in vivo.

OHC somatic displacement in vivo versus in vitro for a change in transmembrane potential

From Eq. 9, Eq. 15 can be simplified as

$$\frac{u_{OHC}}{u_{OHC}^{iso}} = \frac{K_{OHC}}{K_{OHC} + \left(\dfrac{Z_{TR}Z_{BM}}{Z_{TR}+Z_{BM}}\right)}. \tag{19}$$

This quantity is the ratio of in vivo OHC somatic displacement to isolated OHC displacement in response to a given change in transmembrane potential. Fig. 3 shows the amplitude and phase of the ratio derived in Eq. 19. From Fig. 3, the low-frequency amplitude of the ratio is ~0.375 for the parameters used in the figure. At frequencies around the 19 kHz CF at the 3 mm tonotopic location (CF 19 kHz) shown in Fig. 3, the amplitude of the ratio is between 0.9 and 1.5. Note that in this frequency range, the in vivo OHC somatic displacement phase lags the isolated OHC displacement by ~90°.

Although the quantitative values do depend on the parameters used in the figure $(K_{BM} = 10\,K_{OHC}, K_{TR} = 2\,K_{OHC})$, the qualitative behavior demonstrated in Fig. 3 is independent of the parameters used. Even for $(K_{BM} = 50\,K_{OHC}, K_{TR} = 10\,K_{OHC})$, the low-frequency ratio is ~0.1 and the peak value at OoC resonance is 0.45. Therefore, the

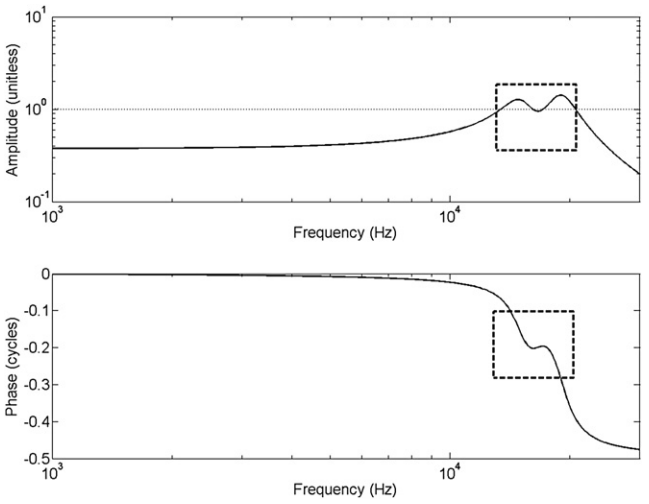

FIGURE 3 This figure shows the amplitude and phase of the ratio of OHC somatic displacement in vivo versus OHC displacement in isolated cells for a given change in transmembrane potential from Eq. 19. The dotted line in the amplitude plot in the upper panel represents a value of 1 for reference. In the boxed region, the in vivo somatic displacement of the OHC approaches the level of isolated OHC displacement in amplitude and is associated with ~90° phase lag. The parameters used in the figure are as follows: $\lambda = 300\ \mu$m is one local wavelength near 19 kHz CF at 3 mm tonotopic location; $N_{OHC} = 53$ (see text) is the number of OHCs. OHC stiffness is derived from Eq. 7 as $K_{OHC} = -\varepsilon N_{OHC}/EMR_{iso}$, where $\varepsilon = -0.1$ nN/mV (37) per OHC, $EMR_{iso} = 20$ nm/mV is the electromechanical ratio for isolated OHC (29). This gives $K_{OHC} = 0.265$ N/m lumped over 300 μm. (Note that this figure is independent of the value of K_{OHC}; see Eq. 19.) Furthermore, the numerical value of K_{OHC} only scales Fig. 2). The BM stiffness is $K_{BM} = 10\ K_{OHC}$ (19) and the RL/TM stiffness is $K_{TR} = 2\ K_{OHC}$. The ratio of BM to TR stiffness is consistent with the in vitro experiments reported in Mammano and Ashmore (51). The BM mass including fluid mass loading on the BM is $M_{BM} = K_{BM}/\omega_{BM}^2$; $\omega_{BM} = 2\pi f_{BM}$; $f_{BM} = 17.5$ kHz. The TM mass (including fluid loading if any) is $M_{TR} = K_{TR}/\omega_{TR}^2$; $\omega_{TR} = 2\pi f_{TR}$; $f_{TR} = 13$ kHz. The BM damping coefficient is $B_{BM} = 2\zeta_{BM}\sqrt{M_{BM}K_{BM}}$ (for $\zeta_{BM} = 0.1$), and the RL/TM damping coefficient is $B_{TR} = 2\zeta_{TR}\sqrt{M_{TR}K_{TR}}$ (for $\zeta_{TR} = 0.1$). For a different parameter set $K_{BM} = 50\ K_{OHC}$, $K_{TR} = 10\ K_{OHC}$, for the same ω_{BM} and ω_{TR}, the low-frequency ratio is ~0.1 and the peak value at OoC resonance is 0.45 with about the same phase as shown in the plot. Therefore, the qualitative results are not sensitive to the parameters used in the plot shown.

qualitative results are not sensitive to the parameters used in Fig. 3. The quantitative results are less sensitive to BM impedance than to RL/TM impedance. This is because the latter is smaller and hence dominates the load impedance $Z_{TR}Z_{BM}/Z_{TR}+Z_{BM}$.

The peaks in the amplitude in Fig. 3 correspond to minima of the effective impedance Z_{eff}^{active} of the OoC (Eq. 16, Fig. 2). The internal resonances in the OoC cause these impedance minima and hence increase the in vivo OHC somatic displacement. The frequencies where the OHC stiffness (*dotted line*) crosses the effective impedance amplitude (*solid line*) in Fig. 2 correspond to frequencies where the ratio in Fig. 3 and Eq. 19 is unit amplitude.

The phase of the ratio shown in the bottom panel of Fig. 3 fluctuates between zero and up to half-cycle lag. (This phase is negative of the phase of the effective impedance shown by a *solid line* in the *bottom panel* of Fig. 2.) The implication of a half-cycle phase lag of the ratio in Eq. 19 and in Fig. 3 is that while a depolarizing transmembrane potential of the OHC leads to contraction in isolated cells, it could lead to elongation (only the electromotility induced component) of OHC in vivo at frequencies much higher than the CF. Around 14–20 kHz (*boxed area* in Fig. 3), the in vivo OHC displacement phase lags the isolated OHC displacement by ~90°. This phase lag means that the electromechanical velocity and force are in-phase, which aids power transfer to the OoC (Eq. 17).

Estimates from in vivo measurements

Deriving OHC and HB displacements

Fig. 4 shows a simplified sketch of the mechanics of the OoC. The sketch shows the transverse and shear components of RL displacement toward ST, and BM displacement toward ST. The difference in the transverse components of the RL and the BM compresses the OHC. The increase in the length of the OHC-Deiters cell (OHC-DC) complex is given by $\Delta L=(u_{BM}-u_{RL})\sin\theta$ (see Fig. 4). Here, θ is the angle made by the RL with vertical. Although DC cup stiffness has not been directly measured yet, it has been estimated to be at least 1000 times stiffer than the OHC (40). Their estimate is based on the presence of microtubules in the DC resembling pillar cells (41,42). Based on this estimate, the displacement of the OHC is well approximated by the displacement of the OHC-DC complex given by ΔL. The contractile displacement of the OHC in vivo is therefore given by

$$u_{OHC}\approx -\Delta L=(u_{RL}-u_{BM})\sin\theta. \tag{20}$$

This OHC displacement is derived from the directly measured RL and BM displacements in sensitive guinea pigs in vivo assuming $\theta=60^\circ$ (based on the geometry, without loss of generality; $\sin 60^\circ=0.87$).

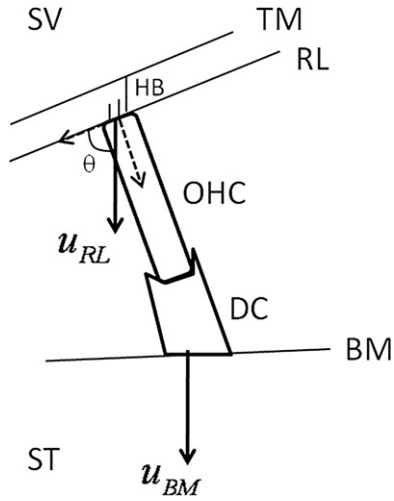

FIGURE 4 Sketch to show the transverse and shear components of RL displacement toward ST and BM displacement toward ST. DC is the Deiters cell. The difference in the transverse components of the RL and the BM compresses the OHC, whereas the RL shear component toward the left as shown displaces the HB in the excitatory direction: HB base moves toward the left, or equivalently HB apex rotates toward the taller stereocilia.

From the classical theory (3), the HB deflection is given by the shear displacement between the TM and the RL. Let us assume that RL shear displacement is larger than that of the TM around the CF. Note that the assumption does not necessarily preclude TM shear resonance. The HB deflection toward excitatory direction is given by

$$u_{HB}=u_{TM}^{right}-u_{RL}^{right}\cong u_{RL}^{left}=u_{RL}\cos\theta. \tag{21}$$

Here, u_{RL} in the last term is the displacement of the RL toward the ST (see Fig.4).

From the measured in vivo data at 19 kHz CF, 40 dB SPL, 3 mm tonotopic location in sensitive guinea pigs from Fig.4 *a* of (27), $u_{RL}=3$ nm and $u_{BM}=1.5$ nm (agrees with (43)), with RL at ~90° phase lead relative to BM. From Eq. 20 and Eq. 21, we get $u_{OHC}=2.9$ nm and $u_{HB}=1.5$ nm. The ratio (amplitude) of OHC displacement to HB excitatory displacement is ~1.93, which is in the same range as measured in isolated cells (44).

Transduction and piezoelectric current

The HB deflection modulates the standing current to produce the alternating transduction current in response to the sound stimulation (20). The transduction current can be represented in the linearized form for small sound levels (36):

$$I_{s1}=(V_{EP}-V_{OHC})G_1u_{HB}. \tag{22}$$

Here, V_{EP} is the endocochlear potential of 80 mV, and V_{OHC} is the resting potential of the OHC equal to about −70 mV for the basal location in guinea pigs. The term G_1 is the

slope of HB conductance versus displacement in vivo. From Fig.1 *F* in Johnson et al. (22),

$$G_1 = \frac{I_{s1}}{(V_{EP} - V_{OHC})u_{HB}} = \frac{2\text{ nA}}{(0 - (-40\text{ mV})) \times 100\text{ nm}} = 0.5\frac{\text{nS}}{\text{nm}},$$

at a somewhat apical location. Here, at the 3 mm tonotopic location, $G_1 = 1$ nS/nm is used (also used in (19)). At 40 dB SPL, $u_{HB} = 1.5$ nm as derived in the previous section. Therefore, the transduction current through a single OHC in vivo around 19 kHz CF at 40 dB SPL is $I_{s1} = 0.225$ nA, which is in the range measured by Johnson et al. (22) and by He et al. (45), after correcting for in vivo conditions as suggested in the supplemental data of Johnson et al. (22).

The total transduction current in the CF-region is given by the product of the single-cell transduction current I_{s1} times the number of OHCs (N_{OHC}) in the region. Near the 19 kHz CP, the wavelength of the traveling wave is ~300 μm, estimating from gerbil measurement in Ren (46) and chinchilla measurement in Narayan and Ruggero (47). The number of OHCs in a 300 μm region is given by 300/17,000 $\times$ 3000 = 53 OHCs, assuming a total of 3000 OHCs in a length of 17 mm for guinea pigs. Therefore, the total transduction current in the 300 μm region is $I^{\lambda}_{s1} = I_{s1} \times N_{OHC} = 11.925$ nA.

The piezoelectric current source I_{s2} due to OHC electromotility for a single OHC (see Fig. 5 and (36)) is

$$I_{s2} = -j\omega\varepsilon_3 u_{OHC}. \quad (23)$$

Here, the radian frequency $\omega = 2\pi f$, where $f = 19$ kHz is the CF of the recording location in the in vivo measurements (27). The term ε_3 is the piezoelectric coupling coefficient equal to -0.1 nN/mV (37). The OHC displacement at 40 dB SPL at the CF derived in the previous section is $u_{OHC} = 2.9$ nm. This gives $I_{s2} = 0.035$ nA for one OHC. The total piezoelectric current over one wavelength is $I^{\lambda}_{s2} = I_{s2} \times N_{OHC} = 1.84$ nA.

OHC transmembrane potential

To estimate the transmembrane and extracellular potentials, consider the electrical circuit shown in Fig. 5. In this figure, φ_{SM} is the potential in the scala media, φ_{OHC} is the potential inside the OHC, φ_{ST} is the potential in the Nuel's space and the ST combined, and $\Delta\varphi_{OHC} = (\varphi_{OHC} - \varphi_{ST})$ is the OHC transmembrane potential. φ_{ST} is also the extracellular potential that would be measured close to the OHC using microelectrodes such as by Fridberger et al. (18). In Fig. 5, R_{ML} is the resistance from scala media to ground and R_{TL} is the resistance from ST to ground. At the 3 mm tonotopic location considered in this article, the resistance R_{ML} is given by the parallel combination of resistance R6 with (R2 + R1)

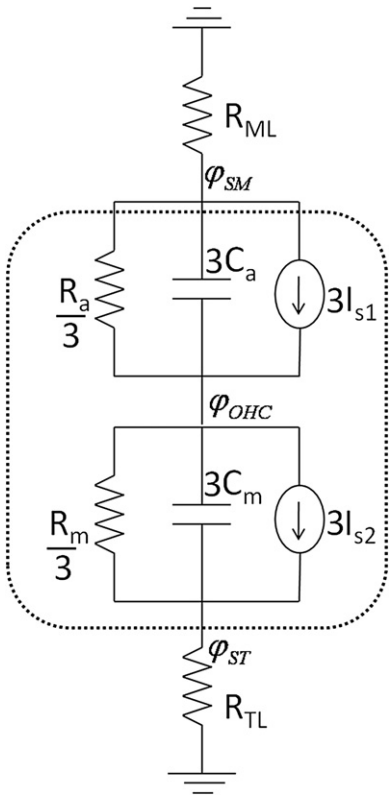

FIGURE 5 Electrical circuit representing a cross section of the cochlea, simplified from Ramamoorthy et al. (36). The dotted box represents the OHCs in the cross section. The resistances R_a and R_m represent the apical and basolateral resistance of a single OHC, C_a and C_m are the apical and basolateral capacitances of a single OHC. R_{ML} is the resistance from scala media to ground and R_{TL} is the resistance from ST to ground. The current source I_{s1} is the transduction current due to HB deflection (Eq. 22) and the current source I_{s2} is the piezoelectric current due to OHC displacement (Eq. 23) per single OHC (see also (36), p. 2762). In Ramamoorthy et al. (36), the current sources due to three OHCs in a single cross section were lumped together. In this figure, the current sources I_{s1} and I_{s2} are for a single OHC—the total number of OHCs is accounted for in the calculations as appropriate.

(48) and is equal to 14 Ωm. The resistance R_{TL} is given by the (R4 + R5) (48) and is equal to 4 Ωm at the 3 mm tonotopic location. Over one wavelength (300 μm), this resistance is $R^{\lambda}_{TL} = 4\ \Omega\text{m}/300\ \mu\text{m} = 13.33\ k\Omega$ and that of the resistance from scala media to ground is $R^{\lambda}_{ML} = 14\ \Omega\text{m}/300\ \mu\text{m} = 46.67\ k\Omega$.

In Fig.5, $Z^{\lambda}_m = 1/(1/R^{\lambda}_m) + j\omega C^{\lambda}_m$ is the basolateral impedance of the OHC over one wavelength and $Z^{\lambda}_a = 1/(1/R^{\lambda}_a) + j\omega C^{\lambda}_a$ is the apical impedance of the OHC over one wavelength. $R_a = 250$ MΩ is the apical resistance of a single OHC using apical conductance of 4 nS per OHC estimated by Karavitaki and Mountain (49), which assumes 50% of the transduction channels are open at rest in vivo. The basolateral resistance R_m of a single OHC is ~0.15 times R_a (17). The effective basolateral resistance of the OHC over one wavelength is given by $R^{\lambda}_m = R_m/N_{OHC} = 0.71$ MΩ. The apical capacitance C_a of a single

OHC is given by the ratio of the time constant of $\tau_a = 0.23$ ms (17) and apical resistance $R_a = 250$ MΩ. This gives $C_a = 0.92$ pF for a single OHC. From Dallos and Evans (17), the basolateral capacitance of a single OHC is $C_m \cong c_a/0.06$, and therefore $C_m = 15.3$ pF. The basolateral capacitance over one wavelength is thus, $C_m^{\lambda} = C_m N_{OHC} = 0.8$ 1n F. The basolateral impedance Z_m^{λ} has a corner frequency of ~275 Hz and RC filter roll-off is seen above that frequency.

Applying Kirchhoff's circuit laws to the electrical circuit shown in Fig. 5 leads to the following equations (ignoring the factor of 3 OHCs per cross section; the total number of OHCs is accounted for later):

$$-\frac{\varphi_{SM}}{R_{ML}} = \frac{\varphi_{ST}}{R_{TL}}, \tag{24}$$

$$\frac{(\varphi_{SM} - \varphi_{OHC})}{Z_a} + I_{s1} = \frac{\varphi_{ST}}{R_{TL}}, \tag{25}$$

$$\frac{(\varphi_{OHC} - \varphi_{ST})}{Z_m} + I_{s2} = \frac{\varphi_{ST}}{R_{TL}}. \tag{26}$$

From Eq. 27, Eq. 25, and Eq. 26, the three potentials can be derived as

$$\varphi_{OHC} = \frac{\left(I_{s1} - \frac{\alpha}{\beta} I_{s2}\right)}{\left(\frac{1}{Z_a} + \frac{\alpha/\beta}{Z_m}\right)}, \quad \varphi_{ST} = \frac{\left(\frac{\varphi_{OHC}}{Z_m} + I_{s2}\right)}{\beta}, \quad \varphi_{SM} = -\frac{R_{ML}}{R_{TL}} \varphi_{ST}, \tag{27}$$

where, α and β are given by

$$\alpha = \left(\frac{1}{R_{TL}} + \frac{R_{ML}/R_{TL}}{Z_a}\right), \quad \beta = \left(\frac{1}{R_{TL}} + \frac{1}{Z_m}\right). \tag{28}$$

The sign of the OHC piezoelectric current I_{s2} relative to the transduction current I_{s1} depends on the in vivo phase of u_{OHC} relative to u_{HB} and is not known at this time. However, I_{s2} is ~7 times smaller than I_{s1} for 19 kHz CF in guinea pigs. Ignoring I_{s2} in Eq. 27 leads to an inaccuracy of <15%. From Eq. 27 and evaluating the parameters over one longitudinal wavelength $\lambda = 300$ μm ($N_{OHC} = 53$), the potentials around 19 kHz CF and 40 dB SPL stimulus are (given in the form $Ae^{j\xi}$ where A is the amplitude and ξ is the phase referenced to I_{s1} or u_{HB}): OHC intracellular potential $\varphi_{OHC} = 0.18\ e^{j(-55/180)\pi}$ mV, extracellular potential exterior to OHC $\varphi_{ST} = 0.14\ e^{j(-18/180)\pi}$ mV, scala media potential $\varphi_{SM} = 0.49\ e^{j(162/180)\pi}$ mV, and the OHC transmembrane potential is $\Delta\varphi_{OHC} = 0.11\ e^{j(-107/180)\pi}$ mV.

In summary, the estimated amplitude of the transmembrane potential over one longitudinal wavelength is 0.11 mV at 19 kHz CF in vivo. This is also the estimated transmembrane potential for a single OHC, because the N_{OHC} OHCs are in parallel. The extracellular potential in the space immediately exterior to the OHC is estimated to be 0.14 mV at 40 dB SPL and 19 kHz. This value is very close to the extracellular potential of 0.15 mV measured by Fridberger et al. (18) at this level and frequency.

It is important to note that the OHC transmembrane potential, which is driven by the transduction current in vivo, depends on the electrical impedance of the basolateral membrane. A smaller time constant per se does not result in larger transmembrane potentials. If the smaller time constant is due to smaller resistance, then the transmembrane potential is reduced up to the cutoff frequency. Above that frequency, however, it is the same as that for the case of the longer time constant because the asymptotic high-frequency response is given solely by the membrane capacitance. This is the case with the measurements reported in Johnson et al. (22). The basolateral impedance derived from (22) is within 2 times the value from (17,30) (and used here) at 19 kHz even though the cutoff frequencies are very different (8 kHz vs. 275 Hz); see Fig. S1 in the Supporting Material. Nevertheless, the larger transduction currents reported by Johnson et al. (22) are important—their Fig. 1 is used to derive parameter G_1 in Eq. 22 in this article. Also important is the change in capacitance that derives from the smaller size of the high frequency hair cells.

Active somatic force

The active force from a single OHC due to its electromotility is given by $F_{OHC}^{active} = \varepsilon \Delta\varphi_{OHC}$. The transmembrane potential amplitude is 0.11 mV at 19 kHz, 40 dB SPL in vivo. Therefore, using $\varepsilon = 0.1$ nN/mV from Iwasa and Adachi (37), the active force on the OHCs over one wavelength is $F_{OHC}^{active,\lambda} = N_{OHC}\varepsilon\Delta\varphi_{OHC} = 0.58\ e^{j(73/180)\pi}$ nN where the 73° phase is relative to u_{HB}. The active force amplitude per OHC is ~11 pN.

The lumped model and estimates from measurements are performed over a 300 μm spatial region near the 3 mm tonotopic location (19 kHz CF) in guinea pigs. All the displacements, currents, and potentials are assumed to have uniform amplitude over the 300 μm region. Because the tuning curve is asymmetric about the CP, this spatial region is skewed to mostly basal to the CP.

In vivo electromechanical ratio

Based on the lumped mechanical model, at the 3 mm tonotopic location, around 19 kHz CF, 40 dB SPL stimulus (see Fig. 3, Eq. 19):

$$\left|\frac{u_{OHC}}{u_{OHC}^{iso}}\right|_{expected} \approx 0.9 - 1.5. \tag{29}$$

For the OHC electromotility to be effective in vivo, it is expected that

$$EMR_{invivo,somatic} = EMR_{iso}\left|\frac{u_{OHC}}{u_{OHC}^{iso}}\right|_{expected} \approx 18 - 30\ \mathrm{nm/mV}. \tag{30}$$

As derived in the previous section, $u_{OHC} = 2.9$ nm at 40 dB SPL and 19 kHz CF from the in vivo measurements and the estimated transmembrane potential in vivo is 0.11 mV. The EMR in vivo is given by

$$EMR_{invivo} = \left|\frac{u_{OHC}}{\Delta\varphi_{OHC}}\right|_{measured} = \frac{2.9\ \mathrm{nm}}{0.11\ \mathrm{mV}} = 26.4\frac{\mathrm{nm}}{\mathrm{mV}}. \tag{31}$$

From Eq. 31 the electromechanical ratio of the OHC in vivo is within the range as expected from Eq. 30. This analysis shows that the measured in vivo OHC displacement could indeed be caused by the estimated a.c. transmembrane potential and thus supports the effectiveness of the electromotility process at this high frequency.

Somatic power in vivo

The average somatic power is given by $P_{somatic}$ = ½ real $(Z_{somatic})|j\omega u_{OHC}|^2$ evaluated over the 300 μm region corresponding to one wavelength at the 3 mm tonotopic location for 40 dB SPL, 19 kHz stimulus. Using OHC displacement of 2.9 nm at this stimulus derived earlier from the measurements of (27) and $Z_{somatic} = Z_{eff}^{active}/j\omega$ =1.56e-6 $e^{j(12.7/180)\pi}$ Ns/m at 19 kHz (which is also very close to its mean value over 14–20 kHz) from Fig. 2, the average somatic power is $P_{somatic}$ = 0.091 pW. (An estimate based on Eq. 17 with the active somatic force also gives 0.095 pW assuming u_{OHC} and u_{HB} are in-phase. It appears to be plausible for u_{OHC} to be in-phase with u_{HB} from Eq. 20 and Eq. 21 and the experimental observation that RL displacement is at least 2 times larger than BM displacement (27) at the location and stimulus considered. However, their relative phase remains to be shown by measurements. This relative phase is not needed for the estimate based on $Z_{somatic}$ given above.)

The average power in BM vibrations, also equal to the average power dissipated (see Methods), is P_{BM} = ½ $B_{bm}|j\omega u_{BM}|^2$ = 0.09 pW, using B_{bm} = 5.6e-6 Ns/m from the parameters listed in the Fig. 2 legend, and 1.5 nm BM displacement at 40 dB SPL and 19 kHz best place (27).

For guinea pigs, the stapes velocity at 104 dB SPL is 125 μm/s at 19 kHz from Fig. 2 of (43), the acoustic input impedance of the cochlea as seen at the stapes is Z_C = 2e11 Ns/m^5 and resistive from Fig. 17 of Puria and Allen (50), and the area of the stapes footplate is A_{st} = 1 mm^2. Thus, for 40 dB SPL, 19 kHz sound stimulus in guinea pig v_{st} = 0.079 μm/s and the estimated average acoustic input power at the stapes is P_{stapes} = ½ real (Z_C) $A_{st}{}^2|v_{st}|^2$ = 6.2e-4 pW.

Thus, the estimated average power in BM vibrations (P_{BM} = 0.09 pW) over one wavelength at the 3 mm location for the 40 dB SPL, 19 kHz stimulus is much greater, by ~22 dB, than the average acoustic input power at the stapes (P_{stapes} = 6.2e-4 pW), which suggests the additional power is from active power sources. The estimated somatic power ($P_{somatic}$ = 0.091 pW) is comparable to the estimated active power in BM vibrations. (This near exact match between the somatic power and the active power in BM vibrations is somewhat unexpected given the approximate nature of these estimates. Nevertheless, the estimates are comparable.)

For the 100 dB SPL, 15 kHz stimulus, the estimated average power in BM vibrations (561 pW; derived from 15 nm BM displacement at 80 dB SPL from Fig. 4 of (27)) is comparable to the average acoustic input power at the stapes (622 pW) suggesting negligible power from active sources at this high stimulus level.

Although these are approximate estimates of the average power—note that the direct measurement of active power in the cochlea is yet to be accomplished—they nevertheless indicate that the predicted somatic power at low stimulus levels could account for the active power in BM vibrations.

DISCUSSION

We propose that the transmembrane potential considered independently is not sufficient to assess the effectiveness of OHC electromotility in vivo. Instead, we propose and evaluate two metrics. One metric is the EMR defined as the amplitude of the ratio of OHC displacement to the change in its transmembrane potential. In isolated OHCs, this ratio is the same as the piezoelectric coefficient. The in vivo EMR estimated from measurements agrees very well with the measured EMR for isolated OHCs after accounting for the effects of the OoC impedances on the OHC somatic displacement in vivo, which is constrained by the impedances of BM on the basal side and RL/TM on the apical side. Despite the RC low-pass filtering, the estimated OHC transmembrane potential of 0.11 mV at 19 kHz (CF) for 40 dB SPL stimulus is sufficient to cause in vivo OHC displacement of 2.9 nm to demonstrate an electromechanical ratio of 26 nm/mV, which is within the expected range for in vivo electromotility (18–30 nm/mV from Eq. 30.). At this stimulus, the estimated somatic force produced by a single OHC is ~11 pN and the estimated total somatic force over one wavelength is 0.58 nN.

Contrary to common understanding, the in vivo OHC somatic displacement is not significantly smaller than the OHC displacement in isolated cells. This is especially the case around and below the CF (~14 kHz to 20 kHz; *boxed area* in Fig. 3), which translates to slightly basal to the CP

applying tonotopic mapping. At these frequencies, the internal resonances of the OoC reduce the effective impedance seen by the somatic force that increases the somatic displacement in vivo. Around the same frequency range, the load impedance seen by the somatic force is approximately conjugate matched with the self-impedance of the OHC (*boxed area* in Fig. 2). This band-limited impedance matching nearly optimizes the OoC to receive maximum power from OHC electromotility. The OHC model presented here can be improved further by including the effects of viscosity, nonlinearity, voltage dependence of OHC stiffness, and a more complex mechanical model of the OoC.

Another more insightful metric is the OHC somatic power in vivo. Our analysis shows that the OoC impedances are nearly optimized for maximum somatic power transfer in vivo challenging the paradigm of maximum (isometric) active force. An approximate quantitative analysis also indicates that the predicted somatic power, if added to the traveling wave, could account for the active power observed in BM vibrations. Our analysis, based on both metrics used to evaluate the recent in vivo measurements from (27), therefore strongly suggests that the OHC electromotility is effective in vivo at high frequencies at basal locations.

SUPPORTING MATERIAL

A figure is available at http://www.biophysj.org/biophysj/supplemental/S0006-3495(11)05471-3.

The authors thank Dr. Kuni Iwasa for critical discussion on the manuscript. The journal reviewers Dr. Anthony Gummer and Dr. William Brownell gave important suggestions that greatly improved the manuscript.

This work was supported by the National Institutes of Health grant NIDCD DC 00141.

Part of this work was presented as a poster at the Mechanics of Hearing Workshop in Williamstown, MA, in July 2011 under the title “Outer hair cell electromotility in vivo”.

REFERENCES

1. Davis, H. 1983. An active process in cochlear mechanics. *Hear. Res.* 9:79–90.
2. Gold, T. 1948. Hearing. II. The physical basis of the action of the cochlea. *Proc. R. Soc. Lond. B. Biol. Sci.* 135:492–498.
3. Dallos, P., A. N. Popper, and R. R. Fay. 1996. The Cochlea. Springer.
4. Lukashkin, A. N., M. N. Walling, and I. J. Russell. 2007. Power amplification in the mammalian cochlea. *Curr. Biol.* 17:1340–1344.
5. Ashmore, J., P. Avan, …, B. Canlon. 2010. The remarkable cochlear amplifier. *Hear. Res.* 266:1–17.
6. Ashmore, J. 2008. Cochlear outer hair cell motility. *Physiol. Rev.* 88:173–210.
7. LeMasurier, M., and P. G. Gillespie. 2005. Hair-cell mechanotransduction and cochlear amplification. *Neuron* 48:403–415.
8. Chan, D. K., and A. J. Hudspeth. 2005. Ca^{2+} current-driven nonlinear amplification by the mammalian cochlea in vitro. *Nat. Neurosci.* 8: 149–155.
9. Dallos, P., X. Wu, …, J. Zuo. 2008. Prestin-based outer hair cell motility is necessary for mammalian cochlear amplification. *Neuron* 58:333–339.
10. Brownell, W. E., C. R. Bader, …, Y. de Ribaupierre. 1985. Evoked mechanical responses of isolated cochlear outer hair cells. *Science* 227:194–196.
11. Dong, X. X., M. Ospeck, and K. H. Iwasa. 2002. Piezoelectric reciprocal relationship of the membrane motor in the cochlear outer hair cell. *Biophys. J.* 82:1254–1259.
12. Frank, G., W. Hemmert, and A. W. Gummer. 1999. Limiting dynamics of high-frequency electromechanical transduction of outer hair cells. *Proc. Natl. Acad. Sci. USA* 96:4420–4425.
13. Santos-Sacchi, J. 1992. On the frequency limit and phase of outer hair cell motility: effects of the membrane filter. *J. Neurosci.* 12:1906–1916.
14. Grosh, K., J. Zheng, …, A. L. Nuttall. 2004. High-frequency electromotile responses in the cochlea. *J. Acoust. Soc. Am.* 115:2178–2184.
15. Gummer, A. W., W. Hemmert, and H. P. Zenner. 1996. Resonant tectorial membrane motion in the inner ear: its crucial role in frequency tuning. *Proc. Natl. Acad. Sci. USA* 93:8727–8732.
16. Lu, T. K., S. Zhak, …, R. Sarpeshkar. 2006. Fast cochlear amplification with slow outer hair cells. *Hear. Res.* 214:45–67.
17. Dallos, P., and B. N. Evans. 1995. High-frequency motility of outer hair cells and the cochlear amplifier. *Science* 267:2006–2009.
18. Fridberger, A., J. B. de Monvel, …, A. Nuttall. 2004. Organ of Corti potentials and the motion of the basilar membrane. *J. Neurosci.* 24:10057–10063.
19. Liao, Z., S. Feng, …, A. A. Spector. 2007. Outer hair cell active force generation in the cochlear environment. *J. Acoust. Soc. Am.* 122:2215–2225.
20. Zidanic, M., and W. E. Brownell. 1990. Fine structure of the intracochlear potential field. I. The silent current. *Biophys. J.* 57:1253–1268.
21. Brownell, W. E., P. B. Manis, …, G. A. Spirou. 1983. Acoustically evoked radial current densities in scala tympani. *J. Acoust. Soc. Am.* 74:792–800.
22. Johnson, S. L., M. Beurg, …, R. Fettiplace. 2011. Prestin-driven cochlear amplification is not limited by the outer hair cell membrane time constant. *Neuron* 70:1143–1154.
23. Ashmore, J. 2011. Pushing the envelope of sound. *Neuron* 70:1021–1022.
24. Brownell, W. E. 1990. Outer hair cell electromotility and otoacoustic emissions. *Ear Hear.* 11:82–92.
25. Iwasa, K. H. 1994. A membrane motor model for the fast motility of the outer hair cell. *J. Acoust. Soc. Am.* 96:2216–2224.
26. Rabbitt, R. D., S. Clifford, K. D. Brenenman, B. Farrell, and W. E. Brownell. 2009. Power efficiency of outer hair cell somatic electromotility. *PLoS Comput. Biol.* 5:e1000444.
27. Chen, F., D. Zha, …, A. L. Nuttall. 2011. A differentially amplified motion in the ear for near-threshold sound detection. *Nat. Neurosci.* 14:770–774.
28. Ashmore, J. F. 1987. A fast motile response in guinea-pig outer hair cells: the cellular basis of the cochlear amplifier. *J. Physiol.* 388:323–347.
29. Santos-Sacchi, J. 1989. Asymmetry in voltage-dependent movements of isolated outer hair cells from the organ of Corti. *J. Neurosci.* 9:2954–2962.
30. Preyer, S., S. Renz, …, A. Gummer. 1996. Receptor potential of outer hair cells isolated from base to apex of the adult guinea-pig cochlea: implications for cochlear tuning mechanisms. *Aud. Neurosci.* 2: 145–157.
31. Lighthill, J. 1981. Energy flow in the cochlea. *J. Fluid Mech.* 106: 149–213.
32. de Boer, E., and A. L. Nuttall. 2000. The mechanical waveform of the basilar membrane. III. Intensity effects. *J. Acoust. Soc. Am.* 107:1497–1507.

33. Olson, E. S. 2001. Intracochlear pressure measurements related to cochlear tuning. *J. Acoust. Soc. Am.* 110:349–367.

34. Shera, C. A. 2007. Laser amplification with a twist: traveling-wave propagation and gain functions from throughout the cochlea. *J. Acoust. Soc. Am.* 122:2738–2758.

35. Deo, N. V., and K. Grosh. 2005. Plified nonlinear outer hair cell models. *J. Acoust. Soc. Am.* 117:2141–2146.

36. Ramamoorthy, S., N. V. Deo, and K. Grosh. 2007. A mechano-electro-acoustical model for the cochlea: response to acoustic stimuli. *J. Acoust. Soc. Am.* 121:2758–2773.

37. Iwasa, K. H., and M. Adachi. 1997. Force generation in the outer hair cell of the cochlea. *Biophys. J.* 73:546–555.

38. Markin, V. S., and A. J. Hudspeth. 1995. Modeling the active process of the cochlea: phase relations, amplification, and spontaneous oscillation. *Biophys. J.* 69:138–147.

39. Liu, Y. W., and S. T. Neely. 2009. Outer hair cell electromechanical properties in a nonlinear piezoelectric model. *J. Acoust. Soc. Am.* 126:751–761.

40. Tolomeo, J. A., and M. C. Holley. 1997. The function of the cytoskeleton in determining the mechanical properties of epithelial cells within the organ of Corti. *In* Diversity in Auditory Mechanics. G. R. L. E. R. Lewis, R. F. Lyon, P. M. Narins, C. R. Steele, and E. Hecht-Poinar, editors.; World Scientific, Singapore. 556–562.

41. Angelborg, C., and H. Engström. 1972. Supporting elements in the organ of Corti. I. Fibrillar structures in the supporting cells of the organ of Corti of mammals. *Acta Otolaryngol. Suppl.* 301: 49–6.

42. Slepecky, N., and S. C. Chamberlain. 1983. Distribution and polarity of actin in inner ear supporting cells. *Hear. Res.* 10:359–370.

43. Zheng, J., S. Ramamoorthy, …, A. Fridberger. 2011. Persistence of past stimulations: storing sounds within the inner ear. *Biophys. J.* 100:1627–1634.

44. Evans, B. N., and P. Dallos. 1993. Stereocilia displacement induced somatic motility of cochlear outer hair cells. *Proc. Natl. Acad. Sci. USA* 90:8347–8351.

45. He, D. Z. Z., S. Jia, and P. Dallos. 2004. Mechanoelectrical transduction of adult outer hair cells studied in a gerbil hemicochlea. *Nature* 429:766–770.

46. Ren, T. 2002. Longitudinal pattern of basilar membrane vibration in the sensitive cochlea. *Proc. Natl. Acad. Sci. USA* 99:17101–17106.

47. Narayan, S. S., and M. A. Ruggero. 2000. Basilar membrane mechanics at the hook region of the chinchilla cochlea. *In* Mechanics of Hearing. H. Wada, T. Takasaka, K. Ikeda, K. Ohyama, and T. Koike, editors.; World Scientific, Singapore. 95–101.

48. Strelioff, D. 1973. A computer simulation of the generation and distribution of cochlear potentials. *J. Acoust. Soc. Am.* 54:620–629.

49. Karavitaki, K. D., and D. C. Mountain. 2007. Imaging electrically evoked micromechanical motion within the organ of corti of the excised gerbil cochlea. *Biophys. J.* 92:3294–3316.

50. Puria, S., and J. B. Allen. 1991. A parametric study of cochlear input impedance. *J. Acoust. Soc. Am.* 89:287–309.

51. Mammano, F., and J. F. Ashmore. 1993. Reverse transduction measured in the isolated cochlea by laser Michelson interferometry. *Nature* 365:838–841.